nature communications

Article

https://doi.org/10.1038/s41467-025-66717-5

Experimental determination of structural motifs of interference-free water undecamer cluster $(H_2O)_{11}$

Received: 20 April 2024

Accepted: 13 November 2025

Published online: 13 December 2025

Check for updates

Tiantong Wang[1,2,7], Yang-Yang Zhang[3,4,7], Shuai Jiang[1,2], Wenhui Yan[1,2], Shangdong Li[1,2], Huijun Zheng[1], Jun-Bo Lu[3], Han-Shi Hu[5], Jiayue Yang[1], Weiqing Zhang[1], Guorong Wu[1], Hua Xie[1], Gang Li[1] ✉, Jun Li[3,4,5] ✉, Ling Jiang[1,2,6] ✉ & Xueming Yang[1,2,4,6]

Structural characterization of archetypal water clusters is essential for exploring the nature of aqueous hydrogen-bonding interactions that are responsible for the properties of water. While spectroscopic measurement of interference-free neutral water clusters has been proven to be challenging due to the difficulty in size selection, recent studies have successfully measured the infrared spectra of small water clusters $(H_2O)_n$ ($n = 2–10$). Thus far, experimental evidence for structural motifs of larger water clusters $(H_2O)_n$ ($n \geq 11$) without environmental perturbation such as an ultraviolet-chromophore label, a messenger tag, or a host matrix has been lacking. Here utilizing the recently-developed size-specific infrared spectroscopy apparatus with a tunable vacuum ultraviolet free electron laser (VUV-FEL) and quantum-chemical studies, we have provided experimental evidence to characterize the structure of interference-free neutral water undecamer $(H_2O)_{11}$. Distinct OH stretching bands provide the evidence for the three lowest-energy isomer families denoted as 515, 43′4, and 55′1 structural motifs. The 515 structure is found to be the dominant one, which features a "5 + 1 + 5" assembling of two stacked 5-membered rings with an additional H_2O on the side. Formation mechanism of these three structural motifs is proposed based on calculated energetics. This work provides crucial insights into the microscopic development of hydrogen-bonding water networks and advances our capabilities toward size-dependence study of a diverse range of neutral hydrated clusters for exploring the stepwise mechanisms of solvation processes such as salt dissolution and acid dissociation.

Water plays an important role in many fields, ranging from geology, environment, biology, to astronomy[1–3]. Water molecules undergo continuous vibration/rotation and hydrogen-bond (HB) rearrangement, forming various complex yet dynamic hydrogen-bonding networks. Structural characterization of liquid water has been proven to be a grand challenge because of its multifaceted, ever-changing patterns of HBs[4]. Inasmuch as the nature of the intermolecular forces between water molecules in water clusters bears resemblance to that in the bulk[5,6], it is crucial to understand the growth patterns of water clusters. As illustrated recently, the studies on hydrated clusters can provide multifaced values to help understanding the bulk properties, e.g., the water coordination structure around hydroxide in the cluster

A full list of affiliations appears at the end of the paper. ✉e-mail: gli@dicp.ac.cn; junli@mail.tsinghua.edu.cn; ljiang@dicp.ac.cn

and aqueous solution is similar[7]; kosmotropic and chaotropic anions change local water structures distinctively different, amplifying the ion-specific effect at the cluster scale[8,9]. Water clusters can be studied by adding one water molecule at a time, which helps to determine the size-dependent development of the structural motifs that are difficult to extract from the condensed-phase experiments[10–17]. Spectroscopic studies of archetypal water clusters thus provided central benchmarks for developing accurate potential functions and universal models of water[18,19].

The structures of small neutral water clusters have been studied experimentally and theoretically. The first transition from two-dimensional (2D) to three-dimensional (3D) structure was experimentally verified at the $(H_2O)_{5\text{-}6}$ region[20–26], the next transition from all-surface to one-water-centered structure was theoretically predicted to occur at $(H_2O)_{17}$[27], and the third transition from one-water-centered to two-water-centered structure was expected at $(H_2O)_{30}$[28]. The largest neutral water cluster for which the precise structure has been experimentally determined without environmental perturbation (i.e., interference-free) is $(H_2O)_{10}$ thus far[29–31]. An undecamer water cluster, $(H_2O)_{11}$, has hence become the long-standing goal of structural characterization for unraveling the cooperative interactions driven by subtle changes in the hydrogen-bonding topology.

Theoretical studies of $(H_2O)_{11}$ predicted 15 different isomer families based on their oxygen framework and hydrogen-bonding topology[32–44]. Quantum-chemical calculations with different methods and basis sets may give different relative energy sequences, which makes it difficult to accurately determine the structures. Structural characterization of $(H_2O)_{11}$ without interference from, e.g., an ultraviolet-chromophore label, a messenger tag, or a host matrix is a cumbersome experimental target, because of difficult size-selection. Infrared-ultraviolet (IR-UV) double resonance spectra of phenol-tagged $(H_2O)_{11}$ suggested the presence of "fused-cube" structures[45]. However, it was unclear whether these structures resulted from the strong attachment of the phenol[16,46].

So far, the structures of interference-free neutral $(H_2O)_{11}$ have not been characterized experimentally. Here, we report a size-specific infrared (IR) spectroscopic study of interference-free neutral $(H_2O)_{11}$ using a scheme based on threshold photoionization with a tunable vacuum ultraviolet free electron laser (VUV-FEL). The agreement between experiment and theory leads us to identify three lowest-energy isomer families that are denoted as 515, 43′4, and 55′1 structures, which feature "5 + 1 + 5", "4 + 3 + 4", and "5 + 5 + 1" assembling of water molecule/cluster pairs, respectively (vide infra). These results provide important insights into the formation and growth mechanism of diverse HB network structures that are responsible for the complex properties of water.

Results

Assignment of IR spectra of the water undecamer

The experimental IR spectrum of $(H_2O)_{11}$ is shown in Fig. 1a. The corresponding band positions are listed in Table 1.

To assign the experimental spectrum and to identify the structures of existing isomers, theoretical studies were carried out to locate the global-minimum structure on the potential energy surfaces and the harmonic vibrational spectra for $(H_2O)_{11}$. The TGMin code with constrained basin-hopping Monte Carlo algorithm[47–49] was used for the global-minimum isomer search, and ab initio MP2/aug-cc-pVDZ (AVDZ) and DLPNO-CCSD(T)/aug-cc-pVTZ (AVTZ) methods were used to calculate the energies and spectra. Our global-minimum structural search found 4521 independent structures for $(H_2O)_{11}$, which identified various low-lying isomers and also cover the previously-calculated isomers[32–44]. As shown in Fig. 2, the structures of the three lowest-energy isomer families for $(H_2O)_{11}$ (labeled 11A (515A-1), 11B (43′4A-1), and 11C (55′1A-1)) are predicted to be nearly isoenergetic within 0.3 kcal/mol at the MP2/AVDZ level, which are consistent with the previous calculations at the MP2/aug-cc-pVTZ and RI-MP2/complete basis set (CBS) levels[40,43]. The nomenclature for the structures of $(H_2O)_{11}$ follows the literature[40,43], in which the individual digits signify the number of water monomers on a given horizontal plane, and the prime indicates that those monomers do not form a closed hydrogen-bond ring. The simulated IR spectra of the 11A, 11B, and 11C isomers are compared with the experimental spectrum in Fig. 1, and the corresponding harmonic vibrational frequencies in the OH stretching region are listed in Supplementary Tables 3–5, respectively. The three lowest-energy isomers of each family and their corresponding IR spectra are representatively illustrated in Supplementary Figs. 10 and 11, respectively.

In the simulated IR spectrum of isomer 11A (Fig. 1c), the four intense bands of single H-donor OH stretching modes (2960, 3116, 3305, and 3352 cm^{-1}, Supplementary Table 3) are consistent with the experimental values (2965, 3117, 3289, and 3343 cm^{-1}, Table 1); the calculated double H-donor OH stretching modes (3394–3583 cm^{-1}) agree with the experimental bands in the spectra range of 3390–3600 cm^{-1}; the predicted bands of H-donor-free OH stretching modes (3699, 3708, and 3716 cm^{-1}) are in excellent agreement with the experimental bands (3701 and 3715 cm^{-1}). Analogously, the simulated IR spectra of isomers 11B and 11 C (Fig. 1d, e and Supplementary Tables 4 and 5) agree with the experimental one (Fig. 1a and Table 1). The best agreement between the experimental and simulated IR spectra is obtained when assuming a ratio of a 1 (11A): 0.8 (11B): 0.5 (11C) mixture of isomers (Fig. 1b), which is consistent with the calculated relative energies. Note that the estimated relative populations of isomers are slightly different from the Boltzmann distribution of an ideal gas (Supplementary Table 6). The simulated IR spectra of the structures of energetically higher isomer families (44′3′A-X) (Supplementary Fig. 11) exhibit some distinct bands that are not observed experimentally, indicative of trivial contribution to the experimental spectrum. Since the low-lying structures of the same isomer family have similar IR spectra due to similar geometries, unambiguous identification of all the other isomers of the 515A, 43′4A, and 55′1A families is cumbrous unless even higher experimental spectroscopic resolution becomes feasible. Thus, it is more rational to analyze the trend of structural motifs for large water clusters.

It can be concluded that the overall agreement of the calculated spectra of the 515A, 43′4A, and 55′1A isomer families with the experimental one is reasonable to confirm the assignment of these three structural motifs responsible for $(H_2O)_{11}$. Note that the simulated intensities of the 2960 cm^{-1} bands (single H-donor OH stretching modes) in the 11A and 11B isomers are much stronger than those in the experimental spectrum. It could be rationalized that the coupling between hydrogen-bond fluctuation and OH stretch broadens the OH stretching band. Furthermore, the fluctuation of single H-donor OH stretching mode is larger than that of double H-donor OH stretching mode. This makes it more difficult to directly compare the simulated and experimental intensities of vibrational bands of hydrogen-bonded molecular clusters, owing to the challenge of theory (anharmonicity, intermolecular zero-point motions, etc.) and the complexity of experiment (IR absorption combined with dissociation, intramolecular vibrational-energy redistribution (IVR), etc.), as reported previously[29,50,51].

The 11A, 11B, and 11C isomers lie within 0.3 kcal/mol of each other, indicating that they can possibly coexist at the finite temperature of experimental conditions. As shown in Fig. 3, our MP2/AVDZ calculation shows that the 11B → 11A isomerization needs going through several transition states and intermediates, with the largest barrier of elementary process of 3.22 kcal/mol. The largest barrier of elementary process for the 11C → 11A isomerization is calculated to be 2.67 kcal/mol at the same theoretical level (Fig. 3). Such barriers might be sufficiently large so that the 11B and 11C isomers could be kinetically trapped by quenching the nonequilibrium species in the soft

https://doi.org/10.1038/s41467-025-66717-5

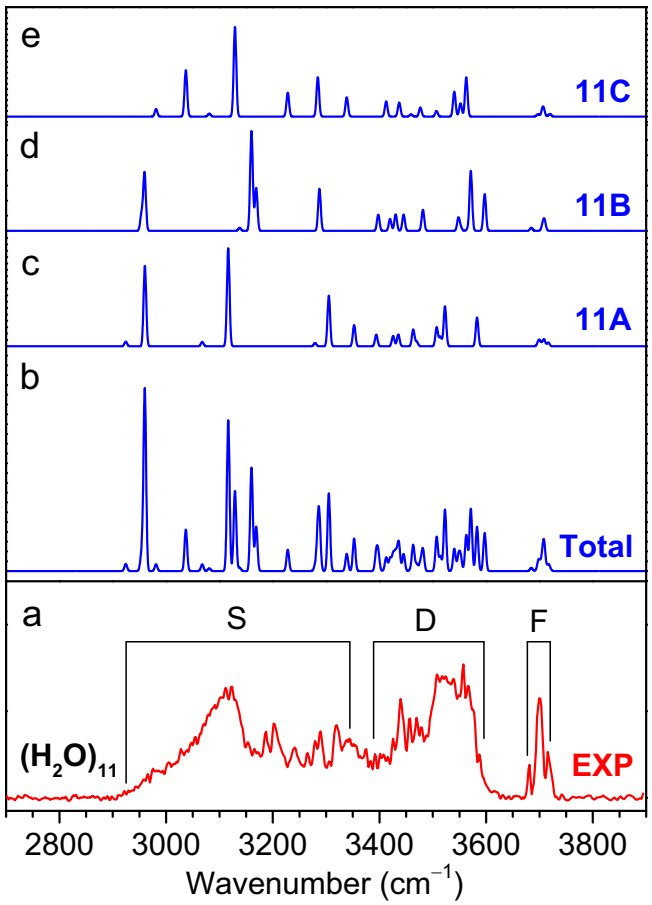

Fig. 1 | Comparison of the experimental and calculated IR spectra of the water undecamer. a Experimental IR spectrum of $(H_2O)_{11}$, where the OH stretching fundamentals assigned to donor-free OH (F), double-donor OH stretch (D), and single-donor OH stretch (S) are indicated. **b** The simulated total IR spectrum of a 1 (11A): 0.8 (11B): 0.5 (11C) mixture of isomers and (**c**–**e**) simulated IR spectrum of each individual isomer, where the calculations were performed at the ab initio MP2/AVDZ level of theory, with the calculated harmonic vibrational frequencies scaled by 0.956.

Table 1 | Experimental vibrational frequencies and band assignments for $(H_2O)_{11}$

Label	Frequency (cm^{-1})	Assignment
	3117	
S	3200	Single H-donor OH stretching modes
	3241	
	3289	
	3319	
	3343	
	3391	
	3401	
D	3439	Double H-donor OH stretching modes
	3507	
	3557	
	3681	
F	3701	H-donor-free OH stretching modes
	3715	

expansion of cold molecular beam[52], which is reminiscent of the observation of low-lying structures of $(H_2O)_n$ ($n = 5$–10) at finite temperature[5,25,26,30,53–55].

To assess the temperature effect on the isomer distribution, Gibbs free energies (ΔG) of isomers 11A, 11B, and 11C were calculated in the temperature range of 0–300 K and the results are shown in Supplementary Fig. 13. It turns out that the calculated free energy difference $\Delta G_{11B\text{-}11A}$ and $\Delta G_{11C\text{-}11A}$ does not vary noticeably below room temperature, indicating that the population of the 11A, 11B, and 11C isomers changes little at low temperature. Furthermore, the 11C isomer becomes the free-energy minimum above 500 K, which is consistent with the previous predictions[43].

Analysis of the electronic structure

To elucidate the nature of the hydrogen-bonding interactions in the water undecamer, the electronic structures of the 11 A, 11B, and 11 C isomers were analyzed with adaptive natural density partitioning (AdNDP)[56], principal interacting orbital (PIO)[57], energy decomposition analysis-natural orbitals for chemical valence (EDA-NOCV)[58], and natural bond orbital (NBO)[59] methods, respectively. The AdNDP and PIO analyses of 11A, 11B and 11C are shown in Supplementary Figs. 14–16 and 17–19, respectively. As pointed out previously[26,60], the HB bonding in the water clusters may be described by a three-center two-electron (3c2e) interaction featuring the delocalization of an adjacent oxygen lone pair (LP(O)) donor to the antibonding σ*(OH) region. Indeed, for 11A, five 3c-2e HB LP(O) → σ*(OH) on the top face, six 3c-2e HB LP(O) → σ*(OH) on the side face, and five 3c-2e HB LP(O) → σ*(OH) on the bottom face are located, as shown in Supplementary Fig. 14.

The contribution of HB to the total bonding in the 11A, 11B, and 11C isomers is predicted to be 96.0%, 95.1%, and 95.1% (Supplementary Table 7), respectively. As shown in Supplementary Figs. 14–16, the AdNDP results reveal extensive delocalized HB interactions in $(H_2O)_{11}$. The total second-order perturbation interaction energy of the 11A, 11B, and 11C isomers is calculated to be 315.25, 312.13, and 304.21kcal/mol (Supplementary Tables 8–10), respectively, which supports the trend of structural stability. The calculated Wiberg bond order (WBO) and natural hybrid orbitals (NHO) of these three isomers (Supplementary Tables 11–13) provide detailed bonding information that agrees well with the atomic distances listed in Supplementary Tables 8–10.

Discussion

The possible presence of the 11A (515A-1), 11B (43′4A-1), and 11C (55′1A-1) isomers in the measured spectra is intriguing, because no experimental evidence for the isomers of interference-free water undecamer has ever been observed. The two nearly-isoenergetic pentagonal prism isomers (10PPD1 and 10PPS1) were identified to be the dominated structures of $(H_2O)_{10}$, which were proposed to be the building blocks for larger hydrogen-bonding networks[30,31]. With this context, structural evolution from $(H_2O)_{10}$ to $(H_2O)_{11}$ is proposed as shown in Fig. 4.

As shown in Fig. 4a, the insertion of the 11th water molecule into a side HB edge of the global-minimum 10PPD1 of $(H_2O)_{10}$ forms the 11A (515A-1) isomer, which features a "5 + 1 + 5" assembling of two stacked 5-membered rings with an additional H_2O on the side. The 11th molecule can also be inserted into a top HB edge of the 10PPD1 isomer of $(H_2O)_{10}$ (Fig. 4a), forming a 11C* structure (55′1-type). The mirror mapping operation of the 11C* isomer yields the 11C (55′1A-1) isomer, which exhibits a "5 + 5 + 1" assembling of water cluster pairs. As shown in Fig. 4b, the 11th water molecule is inserted into a side HB edge of the 10PPS1 isomer of $(H_2O)_{10}$, forming a 11B* structure (43′4A-2), which lies above the global-minimum isomer by 0.12 kcal/mol at the MP2/AVDZ level (Supplementary Fig. 10). The 11B* isomer undergoes the HB in-plane inversion of bottom pentamer to form the 11B isomer, which exhibits a "4 + 3 + 4" assembling of two 4-membered rings connected

https://doi.org/10.1038/s41467-025-66717-5

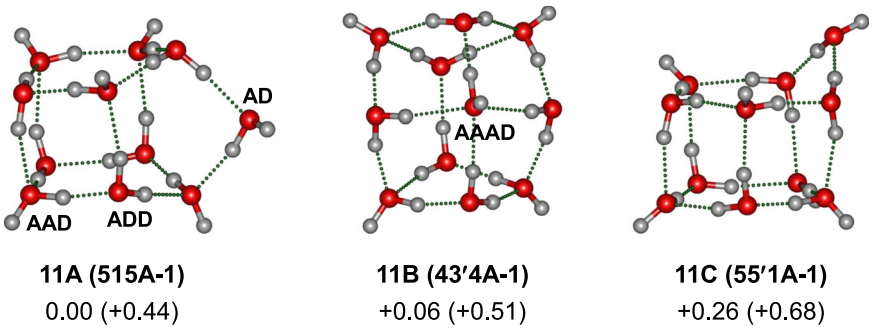

Fig. 2 | Identified structures of $(H_2O)_{11}$ (O, red; H, light gray). Relative energies from MP2/AVDZ and DLPNO-CCSD(T)/AVTZ (in parenthesis) are listed in kcal/mol. The hydrogen-bonding sites are classified as AD, AAD, ADD, and AAAD configurations according to the number of proton-acceptor (A) and proton-donor (D) hydrogen bonds, respectively.

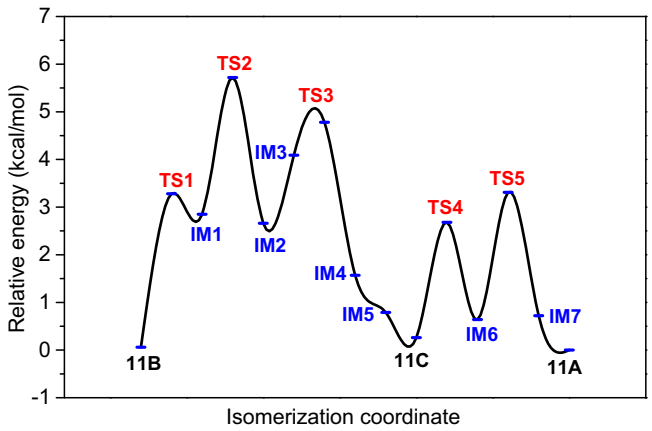

Fig. 3 | Potential energy profiles for the isomerization between 11A, 11B, and 11 C for $(H_2O)_{11}$. Calculations were carried out at the MP2/AVDZ level of theory. The abbreviation "TS" stands for transition state and "IM" for intermediate. The corresponding structures are shown in Supplementary Fig. 12.

by a water trimer chain. As the 515A-1 isomer is predicted to be the global-minimum structure at low temperature, the "5 + 1 + 5" assembling of water cluster pairs appears to be the dominated motif in the development of hydrogen-bonding network structures. These results provide an essential picture of water-pair stacking and a prelude to the diverse structure of liquid water. In contrast, the highly-strained 4-membered ring motif (fused-cube) was assigned for the phenol-tagged $(H_2O)_{11}$ cluster[45], indicative of a pronounced effect of phenol molecule on the influence of the water hydrogen-bonding network. The hydroxy group of phenol forms strong hydrogen bonds with the water molecules, which remarkably tune the internal energy and thereby affect the isomer distribution of water clusters[16,61].

In summary, the VUV-FEL–based size-specific IR spectra of interference-free neutral $(H_2O)_{11}$ are observed for the OH stretches that are very sensitive to hydrogen-bonding environments. We have hereby identified the 515, 43′4, and 55′1 structural motifs of the three lowest-energy isomer families for $(H_2O)_{11}$, which feature "5 + 1 + 5", "4 + 3 + 4", and "5 + 5 + 1" assembling of water cluster pairs, respectively. Along with the previously-observed assembly pattern of "3 + 3" for $(H_2O)_6$, "4 + 4" for $(H_2O)_8$, and "5 + 5" for $(H_2O)_{10}$, the stacking pattern of small-sized water rings exhibits a vital role in the formation of hydrogen-bonding network structures. The present method, which integrates IR spectroscopy with a tunable vacuum ultraviolet free-electron laser and quantum-chemical studies, holds a promise for generalization to size-dependence study of various neutral hydrated clusters for exploring the stepwise mechanisms of solvation processes such as salt dissolution and acid dissociation.

Methods

Experimental methods

The experimental IR spectra of $(H_2O)_{11}$ were measured using a VUV-FEL-based IR spectroscopy apparatus[62]. The water-argon-helium mixture was prepared by using the ultrapure water with resistivity > 18 megohm-centimeters (MΩ-cm). In order to avoid condensation, the operating temperature of the entire gas inlet and the pulsed valve was kept at 353 K. Neutral water clusters were generated by supersonic expansions of a water-argon-helium mixture using a high-pressure pulsed valve (Even-Lavie valve, EL-7-2011-HT-HRR) that is capable of producing very cold molecular beam conditions[63]. The stagnation pressure was approximately 50 bar. The molecular beam passed through a 4 mm diameter skimmer (Beam Dynamics, Model 50.8) and an aperture with 3 mm opening. The extraction plates of reflectron time-of-flight mass spectrometer (TOF-MS) were powered by a high-voltage direct current (DC) of 2950 V. Ionic water clusters were deflected out of the molecular beam by the DC electric field of the extraction plates.

For the vibrational excitation of $(H_2O)_{11}$, we used a tunable IR laser. Subsequent photoionization of $(H_2O)_{11}$ was carried out with ~50 ns delay with a VUV-FEL light at 115.00 nm, forming $(H_2O)_{11}^+$. When the resonant vibrational transition was evoked by the IR laser light and caused vibrational predissociation, a depletion of the selected neutral cluster mass signal can be detected. The IR spectrum of size-selected neutral water cluster $(H_2O)_{11}$ was obtained as a depletion spectrum of the ion signal intensity of $(H_2O)_{11}^+$ as a function of IR wavelength. The VUV-FEL in the present experiment was operated at 20 Hz and IR laser was operated at 10 Hz. IR spectra were recorded in the difference mode of operation (IR laser on−IR laser off). IR and VUV power dependence of the signal was measured to avoid the saturation of vibrational excitation and photoionization. IR spectra were normalized with IR power.

As shown in Supplementary Figs. 1–2 and Supplementary Table 1, the rearrangement of $(H_2O)_{11}^+$ (labeled 11A$^+$) into $[(H_3O)(OH)(H_2O)_9]^+$ (iso 2) need go through several transition states and intermediates, with the largest barrier of elementary process of 4.03 kcal/mol at the MP2/aug-cc-pVDZ (MP2/AVDZ) level of theory. The largest barrier of elementary process for the $[(H_3O)(OH)(H_2O)_9]^+$ (iso 2) → $[(H_3O)(H_2O)_9(OH)]^+$ (iso 1) isomerization is calculated to be 7.37 kcal/mol at the same theoretical level. The calculated rate constant of unimolecular conversion and half-life time of reactant by using reaction path-variational transition state theory (RP-VTST) (Supplementary Table 2) indicate that when the temperature is lower than 80 K, there is a pretty large window of temperature for which the half-life time of the $(H_2O)_{11}^+$ (11 A$^+$) → $[(H_3O)(OH)(H_2O)_9]^+$ (iso 2) and $[(H_3O)(OH)(H_2O)_9]^+$ (iso 2) → $[(H_3O)(H_2O)_9(OH)]^+$ (iso 1) isomerization is longer than the millisecond time scale. The conditions with such temperature are available in the supersonic expansions, because the rotational

https://doi.org/10.1038/s41467-025-66717-5

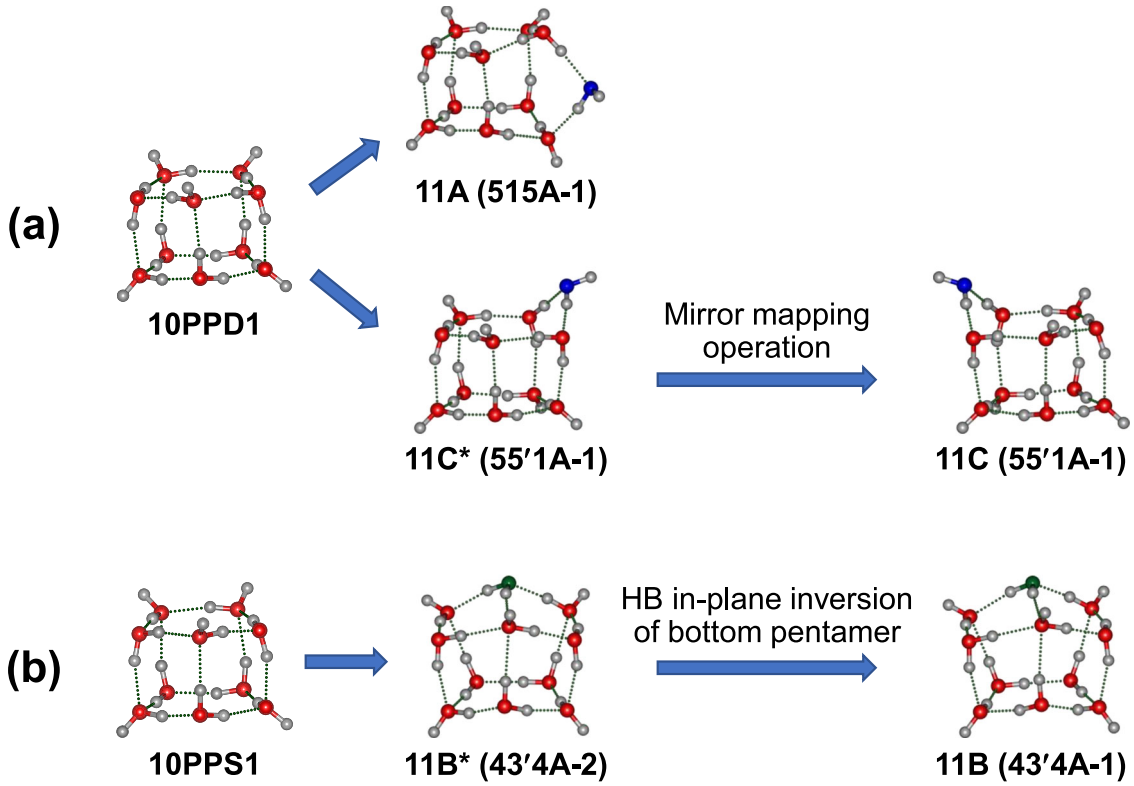

Fig. 4 | A schematic representation of main pathways for the development of hydrogen-bond network structures from $(H_2O)_{10}$ to $(H_2O)_{11}$. a Pathway derived from the 10PPD1 structure of $(H_2O)_{10}$, in which the oxygen atom of the eleventh water molecule is indicated in blue. **b** Pathway derived from the 10PPS1 structure of $(H_2O)_{10}$, in which the oxygen atom of the eleventh water molecule is indicated in green.

temperature of clusters should be less than 10 K and the vibrational temperature could be higher (i.e., a finite temperature)[26,63]. Accordingly, it is reasonable to conclude that the $(H_2O)_{11}^+$ (11 A^+) cluster can reach the time-of-flight mass spectrometer (TOF-MS) detector. These results are consistent with previous observation of the $(H_2O)_n^+$ clusters via the VUV near-threshold photoionization[64–66].

Mass spectra obtained with different VUV wavelengths and beam conditions for neutral water clusters $(H_2O)_n$ ($n = 2–11$) are shown in Supplementary Fig. 3. The assignment of chemical formula of clusters are discussed in Supplementary Information (Supplementary Figs. 4–7). It can be seen from Supplementary Fig. 8 that the intensity of the $(H_2O)_{11}^+$ peak remarkably depletes with IR laser ON (e.g., at 3557 cm^{-1}), whereas that of the $H^+(H_2O)_{11}$ peak does not significantly change. As shown in Supplementary Fig. 9, the IR spectra of each individual cluster $(H_2O)_n$ ($n = 2–11$) are all different from each other, indicating that these IR spectra are free from spectral contamination of larger water clusters, as demonstrated in our previous structural characterization of $(H_2O)_n$ ($n = 2–10$)[26,31,53–55,62].

The tunable VUV-FEL light was generated by the Dalian Coherent Light Source (DCLS) facility. With proper optimization of the LINAC (linear accelerator), a high-quality beam with the emittance down to ~1.5 mm milli-radians, a projected energy spread of ~1%, and a pulse duration of ~1.5 ps can be obtained. An online VUV spectrometer was used to record the spectral characteristics (wavelength, energy, time profile) of every VUV-FEL pulse. The tunable IR laser beam was generated by a Potassium Titanyl Phosphate (KTP)/Potassium Titanyle Arsenate (KTA) optical parametric oscillator/amplifier system (OPO/OPA, LaserVision) pumped by an injection-seeded Nd:YAG laser (Continuum Surelite EX). This system is tunable from 700 to 7000 cm^{-1} with a line width of 1 cm^{-1}. The wavelength of the OPO laser output was calibrated using a commercial wavelength meter (HighFinesse GmbH, WS6-200 VIS IR).

Theoretical methods

Global-minimum structural search based on constrained basin-hopping Monte Carlo algorithm together with quantum-mechanical energies calculated with density functional theory (DFT) was performed for $(H_2O)_{11}$ using TGMin code[47–49]. Quantum chemical calculations with wavefunction theory (WFT) were carried out to refine the energies of the low-lying isomers (within 5 kcal/mol) at the ab initio MP2/ aug-cc-pVDZ (abbreviated as MP2/AVDZ throughout) level using the Gaussian 16 package[67]. Harmonic vibrational frequencies were calculated with analytical second derivatives of the total energy. A scaled factor of 0.956 was used for harmonic vibrational frequencies to account for the systematic errors in the calculations[68]. The resulting stick spectra were convoluted by a Gaussian line shape function with a 6 cm^{-1} full width at half-maximum (FWHM). The MP2/AVDZ relative energies were calculated at 0 K with corrections of zero-point vibrational energies. The single-point ab initio DLPNO-CCSD(T)/aug-cc-pVTZ (AVTZ) relative energies were calculated on the MP2/AVDZ optimized geometries with the ORCA program[69–71], which included the MP2/AVDZ zero-point vibrational energy corrections. Gibbs free energies G(T) = U(T) + PV−TS were calculated with statistical mechanics approach, where U, S, P, V, and T stand for the internal energy, entropy, pressure, volume, and temperature, respectively. Rate constant of unimolecular conversion and half-life time of reactant were calculated by using reaction path-variational transition state theory (RP-VTST) at the MP2/AVDZ level of theory with the GAUSSRATE and POLYRATE programs[72,73].

The nature of the hydrogen bonding interaction in $(H_2O)_{11}$ was analyzed with the natural bond orbital (NBO)[59], adaptive natural density partitioning (AdNDP)[56] and principal interacting orbital (PIO)[57] methods at the MP2/AVDZ level, and the energy decomposition analysis–natural orbitals for chemical valence (EDA-NOCV)[58] method at the DFT level with GGA PBE-D4/TZ2P approach, respectively. The

EDA-NOCV scheme provides both qualitative density ($\Delta\rho_{orb}$) and quantitative energy (ΔE_{orb}) information about the strength and contribution of orbital interactions in chemical bonding, as demonstrated in the study of water clusters $(H_2O)_n$ ($n = 2–10$)[26,31,53–55]. We used the unrelaxed water fragments from the optimized structures to derive the intrinsic binding energies of water clusters.

Data availability

All data needed to support the conclusions of this manuscript are included in the main text or supplementary information. Source data are provided with this paper. All data are also available from the corresponding author upon request. Source data are provided with this paper.

References

1. Stillinger, F. H. Water revisited. *Science* **209**, 451–457 (1980).
2. Gallo, P. et al. Water: a tale of two liquids. *Chem. Rev.* **116**, 7463–7500 (2016).
3. Smith, J. W. & Saykally, R. J. Soft X-ray absorption spectroscopy of liquids and solutions. *Chem. Rev.* **117**, 13909–13934 (2017).
4. Clary, D. C. Quantum dynamics in the smallest water droplet. *Science* **351**, 1267–1268 (2016).
5. Richardson, J. O. et al. Concerted hydrogen-bond breaking by quantum tunneling in the water hexamer prism. *Science* **351**, 1310–1313 (2016).
6. Gora, U., Podeszwa, R., Cencek, W. & Szalewicz, K. Interaction energies of large clusters from many-body expansion. *J. Chem. Phys.* **135**, 224102 (2011).
7. Cao, W., Wen, H., Xantheas, S. S. & Wang, X.-B. The primary gas phase hydration shell of hydroxide. *Sci. Adv.* **9**, eadf4309, (2023).
8. Wen, H., Hou, G.-L., Kathmann, S. M., Valiev, M. & Wang, X.-B. Communication: solute anisotropy effects in hydrated anion and neutral clusters. *J. Chem. Phys.* **138**, 031101 (2013).
9. Valiev, M., Deng, S. H. M. & Wang, X.-B. How anion Chaotrope changes the local structure of eater: insights from photoelectron spectroscopy and theoretical modeling of SCN^- water clusters. *J. Phys. Chem. B* **120**, 1518–1525 (2016).
10. Liu, K., Cruzan, J. D. & Saykally, R. J. Water clusters. *Science* **271**, 929–933 (1996).
11. Buck, U. & Huisken, F. Infrared spectroscopy of size-selected water and methanol clusters. *Chem. Rev.* **100**, 3863–3890 (2000).
12. Keutsch, F. N. & Saykally, R. J. Water clusters: untangling the mysteries of the liquid, one molecule at a time. *Proc. Natl. Acad. Sci. USA* **98**, 10533–10540 (2001).
13. Ludwig, R. Water: From clusters to the bulk. *Angew. Chem. Int. Ed.* **40**, 1808–1827 (2001).
14. Robertson, W. H. & Johnson, M. A. Molecular aspects of halide ion hydration: The cluster approach. *Annu. Rev. Phys. Chem.* **54**, 173–213 (2003).
15. Young, R. M. & Neumark, D. M. Dynamics of solvated electrons in clusters. *Chem. Rev.* **112**, 5553–5577 (2012).
16. Fujii, A. & Mizuse, K. Infrared spectroscopic studies on hydrogen-bonded water networks in gas phase clusters. *Int. Rev. Phys. Chem.* **32**, 266–307 (2013).
17. Heine, N. & Asmis, K. R. Cryogenic ion trap vibrational spectroscopy of hydrogen-bonded clusters relevant to atmospheric chemistry. *Int. Rev. Phys. Chem.* **34**, 1–34 (2015).
18. Babin, V., Medders, G. R. & Paesani, F. Toward a universal water model: first principles simulations from the dimer to the liquid phase. *J. Phys. Chem. Lett.* **3**, 3765–3769 (2012).
19. Samanta, A. K., Wang, Y., Mancini, J. S., Bowman, J. M. & Reisler, H. Energetics and predissociation dynamics of small water, HCl, and mixed HCl-water clusters. *Chem. Rev.* **116**, 4913–4936 (2016).
20. Pribble, R. N. & Zwier, T. S. Size-specific infrared spectra of benzene-$(H_2O)_n$ clusters ($n = 1$ through 7): evidence for noncyclic $(H_2O)_n$ structures. *Science* **265**, 75–79 (1994).
21. Huisken, F., Kaloudis, M. & Kulcke, A. Infrared spectroscopy of small size-selected water clusters. *J. Chem. Phys.* **104**, 17–25 (1996).
22. Liu, K. et al. Characterization of a cage form of the water hexamer. *Nature* **381**, 501–503 (1996).
23. Nauta, K. & Miller, R. E. Formation of cyclic water hexamer in liquid helium: the smallest piece of ice. *Science* **287**, 293–295 (2000).
24. Diken, E. G., Robertson, W. H. & Johnson, M. A. The vibrational spectrum of the neutral $(H_2O)_6$ precursor to the "magic" $(H_2O)_6^-$ cluster anion by argon-mediated, population-modulated electron attachment spectroscopy. *J. Phys. Chem. A* **108**, 64–68 (2004).
25. Perez, C. et al. Structures of cage, prism, and book isomers of water hexamer from broadband rotational spectroscopy. *Science* **336**, 897–901 (2012).
26. Zhang, B. et al. Infrared spectroscopy of neutral water clusters at finite temperature: Evidence for a noncyclic pentamer. *Proc. Natl. Acad. Sci. USA* **117**, 15423–15428 (2020).
27. Lagutschenkov, A., Fanourgakis, G. S., Niedner-Schatteburg, G. & Xantheas, S. S. The spectroscopic signature of the "all-surface" to "internally solvated" structural transition in water clusters in the n = 17-21 size regime. *J. Chem. Phys.* **122**, 194310 (2005).
28. Qian, P., Song, W., Lu, L. & Yang, Z. Ab initio investigation of water clusters $(H_2O)_n$ (n = 2-34). *Int. J. Quantum Chem.* **110**, 1923–1937 (2010).
29. Buck, U., Ettischer, I., Melzer, M., Buch, V. & Sadlej, J. Structure and spectra of three-dimensional $(H_2O)_n$ clusters, n = 8, 9, 10. *Phys. Rev. Lett.* **80**, 2578–2581 (1998).
30. Pérez, C. et al. Hydrogen bond cooperativity and the three-dimensional structures of water nonamers and decamers. *Angew. Chem., Int. Ed.* **53**, 14368–14372 (2014).
31. Zhang, Y.-Y. et al. Spectroscopic and theoretical identifications of two structural motifs of $(H_2O)_{10}$ cluster. *J. Phys. Chem. Lett.* **15**, 3055–3060 (2024).
32. Niesse, J. A. & Mayne, H. R. Global optimization of atomic and molecular clusters using the space-fixed modified genetic algorithm method. *J. Comput. Chem.* **18**, 1233–1244 (1997).
33. Wales, D. J. & Hodges, M. P. Global minima of water clusters $(H_2O)_n$, n <= 21, described by an empirical potential. *Chem. Phys. Lett.* **286**, 65–72 (1998).
34. Sadlej, J. Theoretical study of structure and spectra of cage clusters $(H_2O)_n$, n = 11,12. *Chem. Phys. Lett.* **333**, 485–492 (2001).
35. Upadhyay, D. M., Shukla, M. K. & Mishra, P. C. An ab initio study of water clusters in gas phase and bulk aqueous media: $(H_2O)_n$, n = 1-12. *Int. J. Quantum Chem.* **81**, 90–104 (2001).
36. Maheshwary, S., Patel, N., Sathyamurthy, N., Kulkarni, A. D. & Gadre, S. R. Structure and stability of water clusters $(H_2O)_n$, n = 8-20: an ab initio investigation. *J. Phys. Chem. A* **105**, 10525–10537 (2001).
37. Lee, H. M., Suh, S. B. & Kim, K. S. Structures, energies, and vibrational spectra of water undecamer and dodecamer: an ab initio study. *J. Chem. Phys.* **114**, 10749–10756 (2001).
38. Kabrede, H. & Hentschke, R. Global minima of water clusters $(H_2O)_n$, n <= 25, described by three empirical potentials. *J. Phys. Chem. B* **107**, 3914–3920 (2003).
39. Lenz, A. & Ojamae, L. A theoretical study of water clusters: the relation between hydrogen-bond topology and interaction energy from quantumchemical computations for clusters with up to 22 molecules. *Phys. Chem. Chem. Phys.* **7**, 1905–1911 (2005).
40. Bulusu, S., Yoo, S., Apra, E., Xantheas, S. & Zeng, X. C. Lowest-energy structures of water clusters $(H_2O)_{11}$ and $(H_2O)_{13}$. *J. Phys. Chem. A* **110**, 11781–11784 (2006).
41. Lenz, A. & Ojamae, L. A theoretical study of water equilibria: The cluster distribution versus temperature and pressure for $(H_2O)_n$, n = 1-60, and ice. *J. Chem. Phys.* **131**, 134302 (2009).

42. Miliordos, E. & Xantheas, S. S. An accurate and efficient computational protocol for obtaining the complete basis set limits of the binding energies of water clusters at the MP2 and CCSD(T) levels of theory: application to $(H_2O)_m$, m = 2-6, 8, 11, 16, and 17. *J. Chem. Phys.* **142**, 234303 (2015).
43. Temelso, B. et al. Exploring the rich potential energy surface of $(H_2O)_{11}$ and its physical implications. *J. Chem. Theory Comput.* **14**, 1141–1153 (2018).
44. Rakshit, A., Bandyopadhyay, P., Heindel, J. P. & Xantheas, S. S. Atlas of putative minima and low-lying energy networks of water clusters n = 3-25. *J. Chem. Phys.* **151**, 214307 (2019).
45. Mizuse, K., Hamashima, T. & Fujii, A. Infrared spectroscopy of phenol-$(H_2O)_n$ (n > 10): structural strains in hydrogen bond networks of neutral water clusters. *J. Phys. Chem. A* **113**, 12134–12141 (2009).
46. Buck, U., Pradzynski, C. C., Zeuch, T., Dieterich, J. M. & Hartke, B. A size resolved investigation of large water clusters. *Phys. Chem. Chem. Phys.* **16**, 6859–6871 (2014).
47. Zhao, Y., Chen, X. & Li, J. TGMin: a global-minimum structure search program based on a constrained Basin-Hopping algorithm. *Nano Res* **10**, 3407–3420 (2017).
48. Chen, X., Zhao, Y.-F., Wang, L.-S. & Li, J. Recent progresses of global minimum searches of nanoclusters with a constrained Basin-Hopping algorithm in the TGMin program. *Comput. Theor. Chem.* **1107**, 57–65 (2017).
49. Chen, X., Zhao, Y.-F., Zhang, Y.-Y. & Li, J. TGMin: an efficient global minimum searching program for free and surface-supported clusters. *J. Comput. Chem.* **40**, 1105–1112 (2019).
50. Cole, W. T. S., Farrell, J. D., Wales, D. J. & Saykally, R. J. Structure and torsional dynamics of the water octamer from THz laser spectroscopy near 215 μm. *Science* **352**, 1194–1197 (2016).
51. Jiang, S. et al. Vibrational signature of dynamic coupling of a strong hydrogen bond. *J. Phys. Chem. Lett.* **12**, 2259–2265 (2021).
52. Jordan, K. D. Smallest water clusters supporting the ice I structure. *Proc. Natl. Acad. Sci. USA* **116**, 24383–24385 (2019).
53. Li, G. et al. Infrared spectroscopic study of hydrogen bonding topologies in the smallest ice cube. *Nat. Commun.* **11**, 5449 (2020).
54. Zhang, Y.-Y. et al. Infrared spectroscopic signature of the structural diversity of the water heptamer. *Cell Rep. Phys. Sci.* **3**, 100748 (2022).
55. Zheng, H. et al. Spectroscopic snapshot for neutral water nonamer $(H_2O)_9$: adding a H_2O onto a hydrogen bond-unbroken edge of $(H_2O)_8$. *J. Chem. Phys.* **158**, 014301 (2023).
56. Zubarev, D. Y. & Boldyrev, A. I. Developing paradigms of chemical bonding: adaptive natural density partitioning. *Phys. Chem. Chem. Phys.* **10**, 5207–5217 (2008).
57. Zhang, J.-X., Sheong, F. K. & Lin, Z. Unravelling chemical interactions with principal interacting orbital analysis. *Chem. -Eur. J.* **24**, 9639–9650 (2018).
58. Mitoraj, M. P., Michalak, A. & Ziegler, T. A combined charge and energy decomposition scheme for bond analysis. *J. Chem. Theory Comput.* **5**, 962–975 (2009).
59. Weinhold, F., Landis, C. R. & Glendening, E. D. What is NBO analysis and how is it useful?. *Int. Rev. Phys. Chem.* **35**, 399–440 (2016).
60. Reed, A. E. & Weinhold, F. Natural bond orbital analysis of near-Hartree-Fock water dimer. *J. Chem. Phys.* **78**, 4066–4073 (1983).
61. Tabor, D. P., Kusaka, R., Walsh, P. S., Sibert, E. L. III & Zwier, T. S. Isomer-specific spectroscopy of benzene-$(H_2O)_n$, n = 6,7: Benzene's role in reshaping water's three-dimensional networks. *J. Phys. Chem. Lett.* **6**, 1989–1995 (2015).
62. Zhang, B. et al. Infrared spectroscopy of neutral water dimer based on a tunable vacuum ultraviolet free electron laser. *J. Phys. Chem. Lett.* **11**, 851–855 (2020).
63. Even, U., Jortner, J., Noy, D., Lavie, N. & Cossart-Magos, C. Cooling of large molecules below 1 K and He clusters formation. *J. Chem. Phys.* **112**, 8068–8071 (2000).
64. Tachikawa, H. Ionization dynamics of the small-sized water clusters: a direct ab initio trajectory study. *J. Phys. Chem. A* **108**, 7853–7862 (2004).
65. Belau, L., Wilson, K. R., Leone, S. R. & Ahmed, M. Vacuum ultraviolet (VUV) photoionization of small water clusters. *J. Phys. Chem. A* **111**, 10075–10083 (2007).
66. Garrett, B. C. et al. Role of water in electron-initiated processes and radical chemistry: issues and scientific advances. *Chem. Rev.* **105**, 355–389 (2005).
67. Frisch, M. J. et al. *Gaussian 16, Revision A.03* (Gaussian Inc., 2016).
68. Alecu, I. M., Zheng, J., Zhao, Y. & Truhlar, D. G. Computational thermochemistry: scale factor databases and scale factors for vibrational frequencies obtained from electronic model chemistries. *J. Chem. Theory Comput.* **6**, 2872–2887 (2010).
69. Kendall, R. A., Dunning, T. H. & Harrison, R. J. Electron-affinities of the 1st-row atoms revisited-systematic basis-sets and wave-functions. *J. Chem. Phys.* **96**, 6796–6806 (1992).
70. Weigend, F., Kohn, A. & Hattig, C. Efficient use of the correlation consistent basis sets in resolution of the identity MP2 calculations. *J. Chem. Phys.* **116**, 3175–3183 (2002).
71. Neese, F. The ORCA program system. *Wires Comput. Mol. Sci.* **2**, 73–78 (2012).
72. Zheng, J. et al. *GAUSSRATE (version 2016)* (University of Minnesota, 2016).
73. Frisch, M. J. et al. *POLYRATE (version 2016–2A)* (University of Minnesota, 2016).

Acknowledgements

The authors gratefully acknowledge the staff members of the Dalian Coherent Light Source (31127.02.DCLS) and Specreation Co. Ltd. for technical support and assistance in data collection. We thank Professor Hongjun Fan for helpful discussion. This work was supported by the National Key Research and Development Program of China (2021YFA1400501 to G.L.), the National Natural Science Foundation of China (22125303 to L.J., 22033005 to J.L., 92361302 to L.J., 22103082 to G.L., 22273101 to H.X., 22288201 to L.J., and 21327901 to L.J.), NSFC Center for Single-Atom Catalysis (22388102 to J.L.), the Strategic Priority Research Program of the Chinese Academy of Sciences (XDB0970100 to X.Y.), the Innovation Program for Quantum Science and Technology (2021ZD0303304 to L.J.), the Scientific Instrument Developing Project of the Chinese Academy of Sciences (GJJSTD20220001 to X.Y.), the International Partnership Program of the Chinese Academy of Sciences (121421KYSB20170012 to X.Y.), Dalian Institute of Chemical Physics (DICP I202437 to L.J.), and Guangdong Provincial Key Laboratory of Catalysis (No. 2020B121201002 to J.L.). The computational resource is supported by the Center for Computational Science and Engineering at Southern University of Science and Technology (SUSTech) and the CHEM high-performance supercomputer cluster (CHEM-HPC) located at the Department of Chemistry, SUSTech.

Author contributions

G.L., J.L., and L.J. designed the research. T.W., S.J., W.Y., S.L., H.Z., J.Y., W.Z., G.W., H.X., G.L., L.J., and X.Y. performed the experiments and data analysis. Y.Y.Z., J.B.L., H.S.H., and J.L. performed the theoretical calculations and data analysis. G.L., J.L., and L.J. cowrote the manuscript.

Competing interests

The authors declare no competing interests.

Additional information

Supplementary information The online version contains supplementary material available at https://doi.org/10.1038/s41467-025-66717-5.

Correspondence and requests for materials should be addressed to Gang Li, Jun Li or Ling Jiang.

Peer review information *Nature Communications* thanks Xue-Bin Wang and the other anonymous, reviewer(s) for their contribution to the peer review of this work. A peer review file is available.

[1]State Key Laboratory of Chemical Reaction Dynamics and Dalian Coherent Light Source, Dalian Institute of Chemical Physics, Chinese Academy of Sciences, Dalian, China. [2]University of Chinese Academy of Sciences, Beijing, China. [3]Fundamental Science Center of Rare Earths, Ganjiang Innovation Academy, Chinese Academy of Science, Ganzhou, China. [4]Department of Chemistry and Guangdong Provincial Key Laboratory of Catalytic Chemistry, Southern University of Science and Technology, Shenzhen, China. [5]Department of Chemistry and Engineering Research Center of Advanced Rare-Earth Materials of Ministry of Education, Tsinghua University, Beijing, China. [6]Hefei National Laboratory, Hefei, China. [7]These authors contributed equally: Tiantong Wang, Yang-Yang Zhang. ✉e-mail: gli@dicp.ac.cn; junli@mail.tsinghua.edu.cn; ljiang@dicp.ac.cn